




ORIGINAL ARTICLE

Phosphodiesterase 1 Bridges Glutamate Inputs with NO- and Dopamine-Induced Cyclic Nucleotide Signals in the Striatum

Dahdjim B. Betolngar¹, Élia Mota ¹, Arne Fabritius², Jacob Nielsen³, Charlotte Hougaard³, Claus T. Christoffersen³, Jun Yang⁴, Jan Kehler³, Oliver Griesbeck ², Liliana R.V. Castro ¹ and Pierre Vincent ¹

¹Sorbonne Université, CNRS, Biological Adaptation and Ageing, F-75005 Paris, France, ²Max Planck Institute for Neurobiology, Tools for Bio-Imaging, Am Klopferspitz 18, 82152 Martinsried, Germany, ³H. Lundbeck A/S, Ottiliavej 9, DK-2500 Valby, Denmark and ⁴Shanghai Chempartner Co. Ltd., Shanghai, China

Address correspondence to Pierre Vincent, Sorbonne Université, CNRS, Biological Adaptation and Ageing, Mailbox #256, UMR8256, 7 Quai Saint Bernard, F-75005 Paris, France. Email: pierre.vincent@upmc.fr  orcid.org/0000-0002-8479-1908

Abstract

The calcium-regulated phosphodiesterase 1 (PDE1) family is highly expressed in the brain, but its functional role in neurones is poorly understood. Using the selective PDE1 inhibitor Lu AF64196 and biosensors for cyclic nucleotides including a novel biosensor for cGMP, we analyzed the effect of PDE1 on cAMP and cGMP in individual neurones in brain slices from male newborn mice. Release of caged NMDA triggered a transient increase of intracellular calcium, which was associated with a decrease in cAMP and cGMP in medium spiny neurones in the striatum. Lu AF64196 alone did not increase neuronal cyclic nucleotide levels, but blocked the NMDA-induced reduction in cyclic nucleotides indicating that this was mediated by calcium-activated PDE1. Similar effects were observed in the prefrontal cortex and the hippocampus. Upon corelease of dopamine and NMDA, PDE1 was shown to down-regulate the D₁-receptor mediated increase in cAMP. PDE1 inhibition increased long-term potentiation in rat ventral striatum, showing that PDE1 is implicated in the regulation of synaptic plasticity. Overall, our results show that PDE1 reduces cyclic nucleotide signaling in the context of glutamate and dopamine coincidence. This effect could have a therapeutic value for treating brain disorders related to dysfunctions in dopamine neuromodulation.

Key words: biosensor imaging, calcium, cAMP, cGMP, synaptic plasticity

Introduction

Cyclic nucleotide signaling is an important regulator of neuronal excitability. The intracellular level of cyclic nucleotides is controlled by the balance between synthesis by adenylate and guanylate cyclases (AC and GC), and degradation by 3′/5′-cyclic nucleotide phosphodiesterases (PDEs). There are 11 families of PDEs in mammals that can hydrolyze cAMP and/or cGMP (Keravis & Lugnier 2012). PDE1 hydrolyzes both cAMP and cGMP,

and is the only PDE that is activated by Ca²⁺-calmodulin (CaM) (Hansen & Beavo 1986; Lugnier et al. 1986; Goraya & Cooper 2005), suggesting it can mediate a crosstalk between the intracellular calcium and cyclic nucleotide signaling pathways. In particular, while glutamate increases cGMP production via NMDA receptors and nNOS-dependent NO production (Vallebuona & Raiteri 1995; Piedrafitra et al. 2007; Garthwaite 2019), PDE1 could oppose this effect by promoting cGMP breakdown in such

conditions of elevated calcium. 3 PDE1 genes have been identified (PDE1A-C), which are all expressed in the central nervous system. PDE1A is primarily expressed in CA1–3 of the hippocampus and layer 5–6 of the cortex. PDE1B is highly expressed in the striatum and in the dentate gyrus of the hippocampus. In addition, PDE1B is expressed at lower levels in many other brain areas including the cortex. PDE1C is mostly expressed in the cerebellum (Polli & Kincaid 1994; Yan et al. 1994; Lakics et al. 2010; Kelly et al. 2014). Overall, the expression pattern in the central nervous system is very similar in humans and rodents (Lakics et al. 2010).

Medium-sized spiny neurons (MSNs) are GABA-ergic projection neurons that constitute more than 90% of all neurons in the striatum. They integrate glutamate, nitric oxide and dopamine inputs through the calcium, cGMP and cAMP signaling pathways, respectively. The high expression of PDE1B in these neurons suggests that it plays an important role in the integration of these inputs. MSNs express either D_1 dopamine receptors, or both D_2 dopamine and A_{2A} adenosine receptors, and will be hereafter called D_1 or D_2 MSNs, respectively (Valjent et al. 2009; Bertran-Gonzalez et al. 2010; Yapo et al. 2017). Since PDE1B is reported to be expressed in the majority of striatal neurons (Polli & Kincaid 1994), it is expected to be present in both D_1 and D_2 MSN. Suppression of PDE1B in knockout mice enhanced D_1 -mediated phosphorylation of PKA substrates (Reed et al. 2002), but PDE1B function in D_2 MSNs was not studied. The functional role of PDE1B was confirmed *in vivo*: spontaneous locomotor activity was increased in male and female PDE1B knockout mice (Siuciak et al. 2007), and the induction of locomotor activity by dopamine releasing agents was exacerbated (Reed et al. 2002; Ehrman et al. 2006; Siuciak et al. 2007).

In 6-OHDA lesioned mouse model of Parkinson's disease, increased PDE1B expression was associated with complex changes in cyclic nucleotide signaling (Sancesario et al. 2004), suggesting that PDE1B might be a target for treatment of the disease and the dyskinesias that result from its treatment with levodopa (Giorgi et al. 2008; Sancesario et al. 2014). Although PDEs have been evaluated as therapeutic targets for a wide variety of pathologies (Keravis & Lugnier 2012; Ahmad et al. 2015) including neuropsychiatric disorders (Menniti et al. 2006; Reneerkens et al. 2009; Schmidt 2010), the lack of specificity of early PDE1 inhibitors such as zaprinast and vinpocetine rendered uncertain the actual involvement of PDE1 in the effects reported in preclinical and clinical pharmacological studies (Ahn et al. 1989; Vemulapalli et al. 1996; Sitges & Nekrassov 1999; Sitges et al. 2005; Lugnier 2006; Medina 2011). More recently, selective PDE1 inhibitors have been developed (Maurice et al. 2014): the PDE1 inhibitor ITI-214 was shown to enhance memory processes and cognitive performance (Snyder et al. 2016; Pekcec et al. 2018), while Lu AF64196 was used to examine PDE1 function in the control of vascular smooth muscle cell relaxation (Khammy et al. 2017).

Although these studies have shown an impact of PDE1 modulation on animal behavior, the mechanistic details of its effect remain unclear. Cyclic nucleotide and calcium signals in living neurons are transient and to catch PDE1 in action has been a challenge so far. In this report, we have used biosensor imaging to monitor transient changes in cAMP and cGMP at the single cell level in brain slice preparations. In the first part of this work, the experiments were designed to reveal the action of PDE1 on artificially elevated steady-state cyclic nucleotide levels: a transient increase in intracellular calcium triggered by uncaging NMDA transiently reduced both cAMP and cGMP. We used the recently

developed selective PDE1 inhibitor, Lu AF64196 (Khammy et al. 2017) to show that this effect was mediated by PDE1. The second part of this work shows a functional inhibitory effect of PDE1 on the transient cAMP response to dopamine and on long-term potentiation (LTP). This suggests that PDE1 inhibitors may be useful for treating brain disorders related to dysfunctions in dopamine neuromodulation.

Materials and Methods

Construction of the cyGNAL Biosensor

We synthesized (GeneArt, Thermo Fischer Scientific) the CNB-A and CNB-B region of bovine cGMP dependent protein kinase I alpha (PKG I) *de novo*, starting from residue Q79 to residue K344, analog to (Russwurm et al. 2007), and placed it between different combinations of cyan fluorescent proteins as donors and yellow fluorescent proteins as acceptors in pRSET B (Invitrogen). CNB-B was amplified starting from residue P225 to residue Y335 of PKG I and reinserted inside the sensing domain, replacing CNB-A starting from residue E108 to E211, leaving only a 29 amino acid stretch at the N-terminus of the sensor domain intact.

Recombinant Expression and Protein Purification

Protein over-expression and purification was performed according to the protocol presented in (Fabritius et al. 2018). In brief, His-tagged proteins were over-expressed in E.coli BL21 (Invitrogen) in 50 mL cultures of auto inductive LB. Harvested cells were lysed via physical and enzymatic methods (freeze thaw cycle, lysozyme and sonication) with protease inhibitors (4 mM PMSF, 20 μ g/mL Pepstatin A, 4 μ g/mL Leupeptin, Sigma Aldrich, Germany). It was taken care not to include detergents such as Triton X100 within the purification protocol, as we found this to negatively impact *in vitro* sensor performance. Proteins were then purified from cleared lysate using Ni-NTA agarose resin (Jena Bioscience, Germany) and eluted through completion with imidazole (elution buffer: 20 mM Na_2PO_4 , 300 mM NaCl, 300 mM imidazole).

Biosensor Imaging in Brain Slice Preparations

Mice (C57BL/6J; Janvier labs) were housed under standardized conditions with a 12 h light/dark cycle, stable temperature ($22 \pm 1^\circ\text{C}$), controlled humidity ($55 \pm 10\%$) and food and water *ad libitum*. All animal procedures were performed in accordance with the Sorbonne University animal care committee regulations. Brain slices were prepared from mice aged from 7 to 11 days. Coronal (striatum and hippocampus) and sagittal (prefrontal cortex) brain slices were cut with a VT1200S microtome (Leica). Slices were prepared in an ice-cold solution of the following composition: 125 mM NaCl, 0.4 mM CaCl_2 , 1 mM MgCl_2 , 1.25 mM NaH_2PO_4 , 26 mM NaHCO_3 , 20 mM glucose, 2.5 mM KCl, 5 mM sodium pyruvate, and 1 mM kynurenic acid, saturated with 5% CO_2 and 95% O_2 . The slices were incubated in this solution for 30 min and then placed on a Millicell-CM membrane (Millipore) in culture medium (50% Minimum Essential Medium, 50% Hanks' Balanced Salt Solution, 5.5 g/L glucose, penicillin-streptomycin, Invitrogen). We used the Sindbis virus as a vector to induce expression of the biosensors after overnight incubation (Ehrengruber et al. 1999). The coding sequences of the cAMP biosensor Epac-S^{H150} (Polito et al. 2013), calcium biosensor Twitch-2B (Thestrup et al. 2014) or cGMP biosensor cyGNAL were inserted into the plasmid vector pSinRep5 (Invitrogen, San Diego, CA). The linear pSinRep5 and the DH(26 S)

helper DNA (which contains the structural proteins required for packaging of the Sindbis viral genome) were used to prepare recombinant RNA *in vitro*. The capped and polyadenylated RNA transcripts (from DH26S) and pSinRep5) were co-transfected into BHK cells to produce the pseudovirions. This viral vector was added on the brain slices ($\sim 5 \times 10^5$ particles per slice), and the infected slices were incubated overnight at 35 °C under an atmosphere containing 5% CO₂. Before the experiment, slices were incubated for 30 min in the recording solution (125 mM NaCl, 2 mM CaCl₂, 1 mM MgCl₂, 1.25 mM NaH₂PO₄, 26 mM NaHCO₃, 20 mM glucose, 2.5 mM KCl and 5 mM sodium pyruvate saturated with 5% CO₂ and 95% O₂). Recordings were performed with a continuous perfusion of the same solution at 32 °C.

All experiments were performed in the presence of 200 nM tetrodotoxin (TTX) to block electrical activity. Wide-field images were obtained with an Olympus BX50WI or BX51WI upright microscope with a 40 × 0.8 NA water-immersion objective and an ORCA-AG camera (Hamamatsu). Images were acquired with iVision (Biovision, Exton, PA, USA). The excitation and dichroic filters were D436/20 and 455dcxt. Signals were acquired by alternating the emission filters, HQ480/40 for CFP, and D535/40 for YFP, with a filter wheel (Sutter Instruments, Novato, CA, USA). Filters were obtained from Chroma Technology and Semrock.

Photo-release of caged compounds was performed using high power 360 nm LED sources mounted on the epifluorescence port of the microscopes, providing 14 mW at the exit of the microscope objective (0.5 s flash duration) or 7.5 mW (1 s flash duration). The combination of LED sources at 360 nm (for uncaging) and 420 nm (off-peak light source for 436 nm excitation filter for imaging) was purchased from Mightex (Toronto, Canada). The frequency of data acquisition, usually 1 image pair every 30/50 s, was increased to 0.6 Hz in order to resolve peak dynamics, starting 10 data points before MNI-NMDA and/or NPEC-DA uncaging.

Image Analysis

Images were analyzed with custom routines written in the IGOR Pro environment (Wavemetrics, Lake Oswego, OR, USA). No correction for bleed-through or direct excitation of the acceptor was applied to keep the benefit of ratiometric cancellation of optical artefacts. Biosensor activation level was quantified by ratiometric imaging: donor fluorescence divided by acceptor fluorescence for Epac-S^{H150} and cyGAL; acceptor divided by donor for Twitch-2B. The emission ratio was calculated for each pixel and displayed in pseudocolor images, with the ratio value coded in hue and the fluorescence of the preparation coded in intensity. Wide-field imaging of Epac-S^{H150} allowed for the separation of D1 and D2 MSNs, provided that the infection level was kept low and no fluorescence overlap between neighboring neurones was observed. The optical cross-contamination resulting from out of focus light was evaluated by the response to CGS 21680, an agonist of the adenosine A_{2A} receptors, and SKF-81297, a selective agonist of dopamine D₁ receptors: cells were rejected from analysis if the cross-contamination was above 30%. Cells were also excluded from the analysis when basal ratio was elevated, when the response to forskolin was lacking or when the neuronal morphology was altered (uneven cell contours).

LTP Measurements

Male Wistar rats (7–9 weeks old) from Shanghai Laboratory Animal Center (Shanghai, China) were used. The rats were

housed under 12 h light/dark cycle at a temperature of 23 ± 3 °C and a humidity of 40–70%. Food and water was available *ad libitum*. All procedures were conducted with approval from the Danish Animal Experimentation Inspectorate (journal no. 2014 15 0201 00 339) and in accordance with the ChemPartner Institutional Animal Care and Use Committee. Rats were anesthetized by isoflurane and perfused transcardially with an ice-cold sucrose saline solution (in mM): 110 sucrose, 60 NaCl, 3 KCl, 28 NaHCO₃, 1.25 NaH₂PO₄, 0.5 CaCl₂, 7 MgCl₂ and 5 glucose (pH 7.4; saturated with 95% O₂/5% CO₂). After decapitation, brains were removed, placed in chilled sucrose solution and parasagittal slices (350 μm) containing the Nucleus Accumbens (NAc) were cut using a VT1200S vibratome (Leica Microsystems Inc., Bannockburn, Illinois, USA). Slices were incubated in regular artificial cerebrospinal fluid (ACSF) containing (in mM): 119 NaCl, 2.5 KCl, 1.2 Na₂HPO₄, 25 NaHCO₃, 2.5 CaCl₂, 1.3 MgCl₂ and 10 glucose (pH 7.4; saturated with 95% O₂/5% CO₂) at 30 °C for the first 60 min and then transferred to room temperature prior to recordings.

Multi-electrode array (MEA) MED64 Quad 2 systems (AlphaMed Scientific, Japan) were used for extracellular recordings. The MEA probes were composed of 16 platinum electrodes on the surface of a carrier substrate. The electrodes (each 50 × 50 μm²) were arranged in a 4 × 4 matrix, 150 μm apart from each other. Slices were left in the probe for at least 30 min prior to recordings and continuously perfused with oxygenated ACSF (4 mL/min, 32 °C). In most recordings, the synaptically evoked population spike/field excitatory postsynaptic potential (fEPSP, N₂) which is mediated by endogenous glutamate release and concomitant activation of AMPA receptors, was preceded by a nonsynaptic compound action potential (N₁) that is independent of glutamate release and activation of glutamate receptors. fEPSPs were obtained in the presence of the GABA_A antagonist Gabazine (SR95531, 10 μM). 0–80 μA biphasic pulses (100 μs each) with a 5 μA step were applied to evoke fEPSPs and input/output relations were measured. The stimulation intensity evoking a half-maximal response was used for LTP experiments. Electrical stimulation was applied at the NAc core, 100–400 μm from the border between the cortex and the NAc core, to stimulate primarily infralimbic and prelimbic afferents. fEPSPs were recorded from a neighboring electrode 150 μm caudal of the stimulation electrode and reported as fEPSP slopes (10–90% of the rising phase of the response).

Following a 30 min-long stable baseline recording, slices were exposed to either DMSO (control) or 3 μM Lu AF64196 for the remaining of the experiments. And 30 min after DMSO or Lu AF64196 application, LTP was induced by applying a theta burst stimulation (TBS) (Hawes et al. 2013): 10 bursts were delivered at 200 ms interval—each burst consisting of 4 pulses delivered at 50 Hz. The protocol was repeated 10 times at 15 s intervals.

Drugs

Solutions were prepared from powders purchased from Sigma-Aldrich (St Quentin-Fallavier, Isère, France). TTX was from Latoxan (Valence, France). All other drugs were from Tocris Bio-technique (Lille, France). NPEC-DA: (N)-1-(2-nitrophenyl)methyl-carboxy-3,4-dihydroxyphenethylamine. MNI-NMDA: 4-methoxy-7-nitroindolyl-caged N-methyl-D-aspartic acid. DEANO: 2-(N,N-diethylamino)-diazepam 2-oxide sodium salt hydrate.

SKF-81297, a selective agonist of dopamine D₁ receptors, was used to identify MSNs of the D1 type, while CGS 21680, an agonist of the adenosine A_{2A} receptors was used to identify MSNs of the D2 type (Fig. 3). All drugs except TTX and

DEDMSO were added to the bath solution from a stock solution in DMSO; final DMSO concentration in the bath solution remained below 1%.

Statistical Analysis

For biosensor imaging experiments, the responses obtained from all neurons were averaged together and statistics were calculated per experiment (i.e., brain slice). N indicates the number of repeats of the same experiment, and n indicates the total number of neurons. Statistical analysis (unpaired t-tests, except for data in Fig. 6 where paired t-test was used) were performed using Igor Pro (Wavemetrics, Lake Oswego, OR, USA). Degrees of freedom were calculated assuming a possible difference in variance between the samples, resulting in noninteger degrees of freedom values (reported between brackets). For LTP quantification, statistics were calculated per cell, assuming a same variance for all samples. Shading on traces represent standard error of the mean (SEM).

Results

A New Biosensor for cGMP

Several existing FRET biosensors for cGMP are based on dim fluorescent proteins, usually CFP and YFP, or display a limited cGMP selectivity, therefore limiting their use in living cells (Russwurm & Koesling 2018), and we therefore undertook the development of a novel fluorescence resonance energy transfer (FRET) biosensor for optimal measurement of changes in intracellular cGMP in brain slice preparations. We selected the cGMP binding domain of the bovine PKG I. Even though CNB-A of PKG I has high affinity to cGMP, it only displays poor selectivity between cGMP and cAMP (Kim et al. 2011; Huang et al. 2014). We reasoned that under physiological conditions, given comparatively high cAMP concentrations, CNB-A would not contribute much to the required conformational change within the FRET sensor, because its binding site would be saturated. We therefore replaced the CNB-A binding site within the sensor with a copy of the structurally very similar CNB-B binding site, leading to a tandem of CNB-B domains with a high selectivity for cGMP over cAMP. In our hands, sensors using 2 CNB-B binding sites displayed a 2-fold increase in response over sensors using CNB-A and CNB-B binding sites.

We incorporated the brightest available fluorescent proteins in the relevant wavelength ranges, namely mCerulean3 (Markwardt et al. 2011) as the donor and Ypet (Nguyen & Daugherty 2005) as the acceptor fluorescent proteins. We optimized the positioning of fluorescent proteins within the sensor and found that the best overall performance was achieved by having mCerulean3 in a C-terminal position and by removing 11 amino acids from the C-terminus of a N-terminally positioned Ypet (Fig. 1A). This novel biosensor, called cyGNAL, is responding to an increase in cGMP with an inverted change in donor and acceptor fluorescence (Fig. 1B), indicative of a decreased FRET upon cGMP binding. This is similar to the effect of cAMP on T Epac^{vv} and the Epac-S^H series (Polito et al. 2013; Klarenbeek et al. 2011, 2015). The dose-response curve of cyGNAL for cGMP could be fitted to a Hill equation with a K_d of 465 ± 69 nM and a Hill coefficient of 0.801 ± 0.075 , while the dose-response curve for cAMP showed an EC_{50} in the millimolar range (Fig. 1C). This biosensor thus shows a large selectivity for cGMP against cAMP. The ratio was stable at physiological pH and displayed an increase in ratio below 7 (Fig. 1D). Since

the fluorophores have a pK_a in a much lower range, this suggests a pH sensitivity in other domains of the protein.

The properties of the biosensor were further tested in brain slice preparations using viral transfer. In striatal medium spiny neurons, cGMP elevation by bath application of the NO donor DEANO (10 μ M) produced a steady-state F480/F535 ratio increase in all recorded striatal neurons as expected. This response was not saturating since application of the nonspecific PDE inhibitor IBMX at the end of the recording increased the ratio further to a higher steady-state level (Fig. 1E). As commonly accepted (Russwurm & Koesling 2018), we assumed this final level to correspond to biosensor maximal response, that is, saturation of the biosensor with cGMP.

NMDA Receptor Activation Transiently Decreases cGMP in the Striatum

Since PDE1 is highly expressed in the striatum, we first examined its functional role in the control of cGMP in striatal slices in which the cyGNAL biosensor was sparsely expressed via viral transduction. To reduce variability resulting from endogenous electrical activity in the brain slice, action potentials were suppressed by the continuous application of TTX (200 nM) in all experiments. As previously described, tonic production of cGMP is low in slices at basal conditions (Polito et al. 2013) and cGMP production was first increased to a higher steady-state level by applying the NO donor DEANO (10 μ M). PDE1 activity is calcium dependent, and we aimed at increasing intracellular calcium with a transient activation of NMDA receptors while monitoring changes in intracellular cGMP (Fig. 2A,B). To this end, a caged-derivative of NMDA, MNI-NMDA (100 μ M), was applied during the steady-state cGMP level, which had no effect by itself. After a few minutes to allow for the diffusion of the compound into the brain slice, the uncaging protocol was performed: acquisition frequency was increased to 0.6 Hz and a flash of UV light was applied to release NMDA in the brain slice. Immediately following the flash, the cGMP level showed a multiphasic change with an initial decrease for about 1 min, then a recovery overshooting the initial level and finally a progressive return to the level before uncaging after 3 min (Fig. 2B). At the end of the recording, the nonselective PDE inhibitor IBMX (200 μ M) was added to reach the maximal ratio response of the biosensor, and that level was used for normalization. PDE9A which is not inhibited by IBMX and expressed at a low level in the brain, has low K_m and V_{max} for cGMP (Rybalkin et al. 2013; Dornier-Ciossek et al. 2017) and therefore unlikely to prevent reaching the saturation level of the biosensor in that final condition. The decrease in ratio value after MNI-NMDA uncaging was of $-41.8 \pm 8.5\%$ (mean \pm SD, $N = 5$, $n = 38$) of the maximal ratio response.

To check for photophysical effects of the UV flash on the biosensor, the same experiment was performed in the absence of MNI-NMDA; this had negligible effect (Supplementary Fig. S1A). To control whether MNI-NMDA exerted effects independently of NMDA receptors upon uncaging, the same experiment was performed in the presence of the NMDA receptor antagonist D-APV (40 μ M), which strongly reduced the effect of MNI-NMDA uncaging (Supplementary Fig. S1B).

With each molecule of biosensor binding 2 molecules of cGMP, it might be possible that the biosensor exerts a buffering effect on the response to be measured. To test for this effect, the fluorescence emission of the YFP channel in baseline condition was used as a proxy for biosensor concentration and was measured for every neuron that was well in focus, measuring

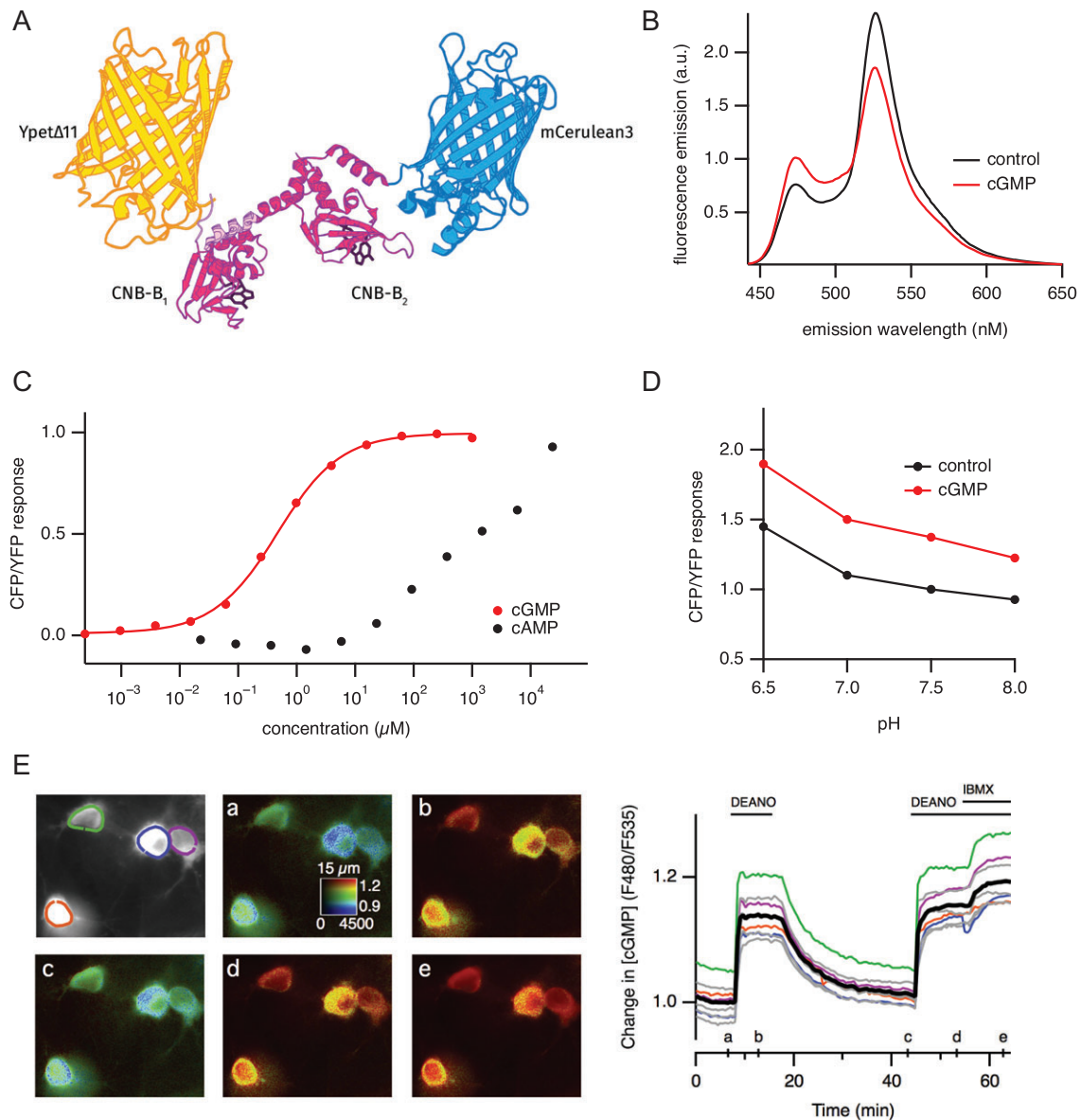


Figure 1. A novel biosensor for imaging cGMP. (A) Structure of the FRET-based cGMP sensor cyGNAL. The sensor domain is constituted of a tandem of the CNB-B domain from bovine type I PKG placed in between Ypet Δ 11 (acceptor) and mCerulean3 (donor). (B) Emission spectrum of cyGNAL without (control) and with 1 mM cGMP. (C) cGMP and cAMP titration of the ratio response. The cGMP curve is fitted to a Hill equation with a K_d of $0.465 \pm 0.069 \mu\text{M}$ and a Hill coefficient of 0.801 ± 0.075 . Half-maximal activation of cyGNAL was obtained with a concentration of 1.4 mM cAMP. (D) pH dependency of the ratio in control condition or with 1 mM cGMP. (E) The cyGNAL biosensor was expressed in striatal brain slices and imaged with wide-field microscopy. Raw fluorescence of the acceptor is displayed in gray and donor/acceptor fluorescence ratio is displayed in pseudocolor, coded from blue (low F480/F535 ratio, i.e., low cGMP) to red (high cGMP). Ratio images (a–e) correspond to the time points indicated in the bottom graph. Changes in ratio were measured during time and plotted besides: each trace indicates the F480/F535 emission ratio measurement on regions indicated by the color contour drawn on the gray image. Gray traces correspond to regions of interest outside this region of the image. The thick black trace represents the average. Horizontal bars indicate the bath application of DEANO (10 μM) and IBMX (200 μM).

the average fluorescence intensity of the 10% brightest pixels in the region of interest. Supplementary Figure S2A shows all the responses to NMDA uncaging with a color coding that reflects fluorescence intensity. Intensity values cover a range from 4 to 120 counts/pixel/s. There is no overt relationship between fluorescence intensity and the shape of the NMDA-induced decreases in cGMP concentration. The amplitude of negative peak and onset slope plotted against fluorescence intensity (Supplementary Fig. S2B and C) show a tendency towards response of smaller amplitude and slower onset for the highest

biosensor expression levels. However, this tendency appears modest, and affects only a minority of neurones.

We then used the selective PDE1 inhibitor Lu AF64196 (Khammy et al. 2017) to determine the contribution of PDE1 on the change in cGMP level induced by NMDA uncaging (Fig. 2C). The addition of 10 μM Lu AF64196 to DEANO had no effect on the steady-state cGMP levels, showing that PDE1 does not control cGMP in that condition. However, Lu AF64196 suppressed the transient decrease observed with NMDA uncaging: in the presence of 10 μM Lu AF64196, the ratio decrease in response to

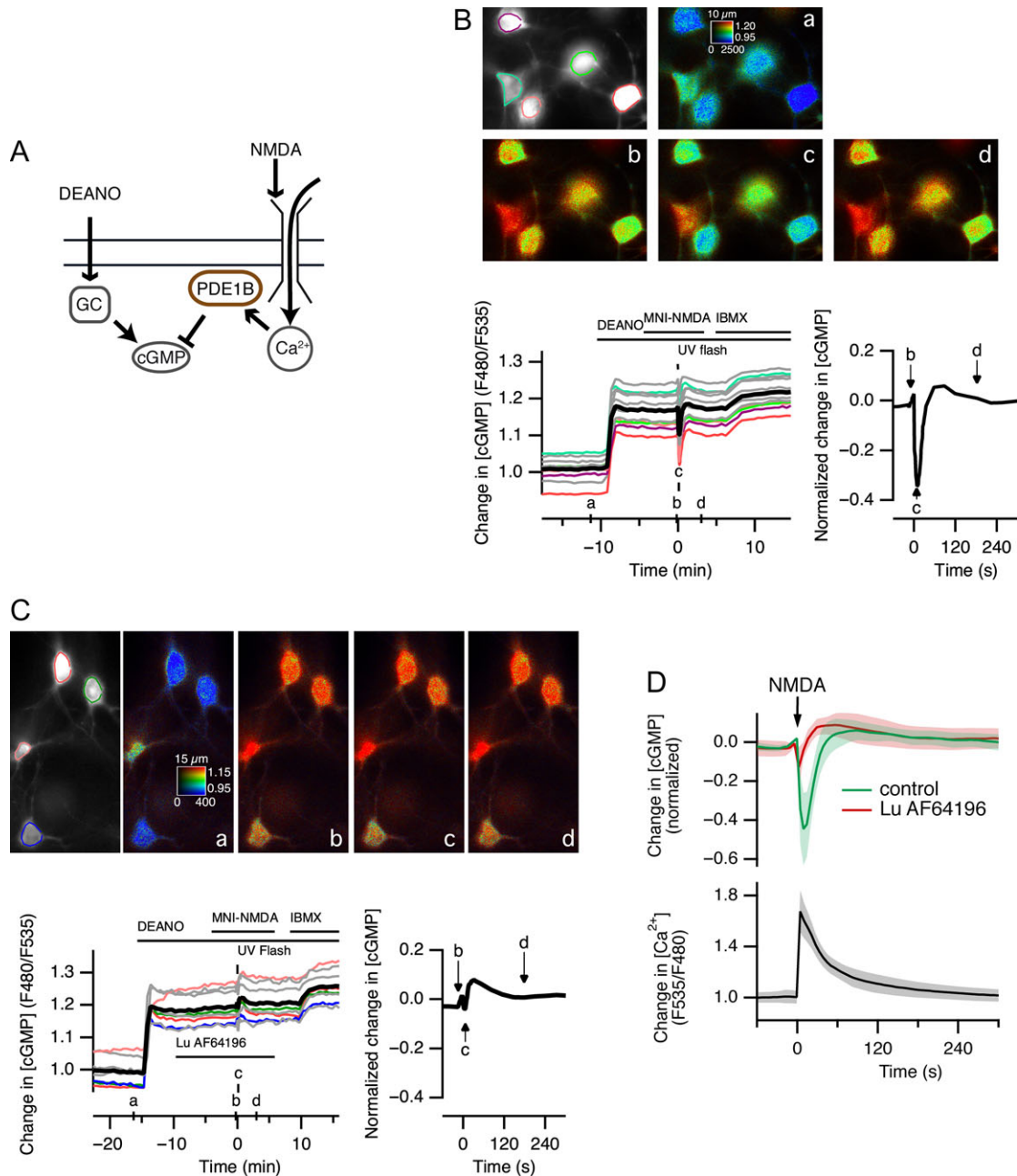


Figure 2. NMDA uncaging transiently decreases cGMP in striatal neurons, in a PDE1 dependent manner. (A) DEANO (10 μ M) was applied to activate the soluble cyclase and trigger cGMP production. NMDA was released from caged NMDA (MNI-NMDA, 100 μ M) by a flash of UV light. NMDA receptors allow for a calcium influx that activates PDE1. (B) Wide-field imaging of mouse striatal brain slices expressing the cyGNA1 biosensor for cGMP. Raw fluorescence of the acceptor is displayed in gray and donor/acceptor fluorescence ratio is displayed in pseudocolor, coded from blue (low F480/F535 ratio, i.e., low cGMP) to red (high cGMP). Changes in ratio are plotted below, left: each trace indicates the F535/F480 emission ratio measured over the region of interest of corresponding color shown on the gray image. Traces in gray correspond to regions of interest outside the displayed part of the field. The black trace represents the average. Drugs were applied in the bath for the duration indicated by the horizontal bars. Ratio images correspond to the time points indicated on the horizontal axis. The graph on the right shows the normalized average ratio change for all the regions of interest in this experiment. Time 0 was the time of the UV flash; amplitude 0 is the average of the 10 data points that precede the UV flash; the ratio was normalized to the maximal ratio change obtained with DEANO plus IBMX (200 μ M). (C) Same as (B) except that 10 μ M Lu AF64196 was applied before and during NMDA uncaging. (D) Similar experiments were averaged, with shading indicating SEM. Top: Response to NMDA uncaging measured with the cyGNA1 biosensor for cGMP in control condition (green: $n = 33$, $N = 4$) and in the presence of 10 μ M Lu AF64196 (red: $n = 48$, $N = 6$). Bottom: changes in intracellular calcium during the same NMDA uncaging protocol measured with Twitch-2B (black: $n = 37$; $N = 3$).

the UV flash was $-3.3 \pm 4.3\%$ (mean \pm SD, $N = 6$, $n = 47$) of the maximal ratio response, similar to the response obtained in the absence of MNI-NMDA or with NMDA receptor antagonists, and significantly different from the control response in the absence of the inhibitor ($t[3.4] = 5.7$, $P = 0.007$, Fig. 2D, top traces).

In the presence of 10 μ M DEANO and before the flash of UV light, the steady-state ratio value measured with the cyGNA1 biosensor was $79.6 \pm 5.3\%$ (mean \pm SD, $N = 12$, $n = 89$) of the maximal ratio response; considering the K_d and Hill coefficient described for the cyGNA1 biosensor, this level corresponds to a

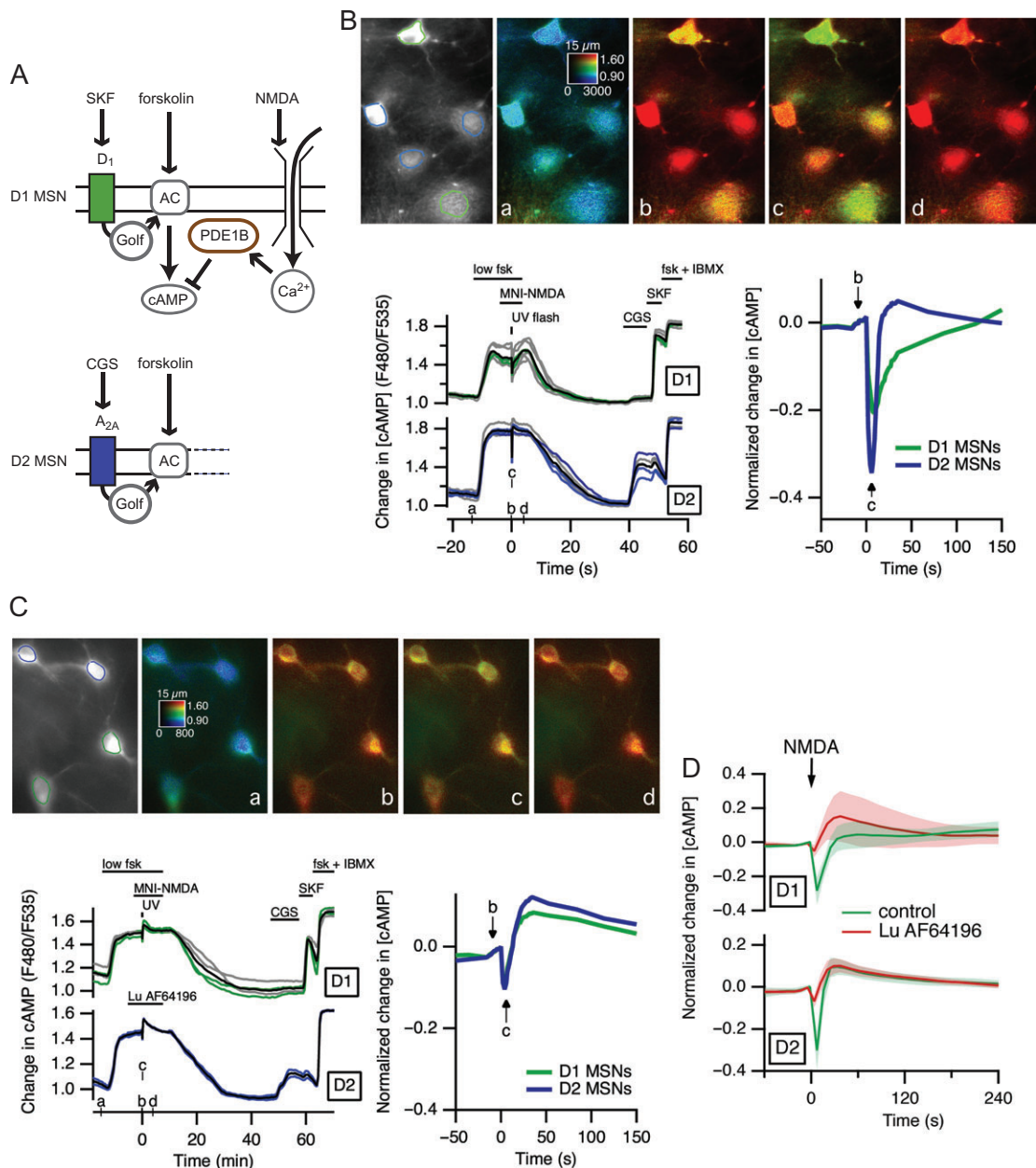


Figure 3. NMDA uncaging transiently decreases cAMP in striatal neurons, an effect blocked by the PDE1 inhibitor Lu AF64196. (A) A low concentration of forskolin (500 nM) was used to sub-maximally activate cAMP production. NMDA was released from caged NMDA (MNI-NMDA, 100 μM) by a flash of UV light, triggering a calcium influx to activate PDE1. MSNs were identified as D1 or D2 from their response to either SKF-81297 (SKF, 1 μM, agonist of D1 dopamine receptors) or CGS 21680 (CGS, 1 μM, A_{2A} adenosine receptor). Maximal ratio was determined at the end of the experiment using 13 μM forskolin and 200 μM IBMX. (B) Wide-field imaging of mouse striatal brain slices expressing the Epac-S^{H150} biosensor for cAMP. Raw fluorescence of the acceptor is displayed in gray and donor/acceptor fluorescence ratio is displayed in pseudocolor, coded from blue (low F480/F535 ratio, i.e., low cAMP) to red (high cAMP). Changes in ratio are plotted below, left: each trace indicates the F480/F535 emission ratio measured over the region of interest of corresponding color shown on the gray image. Traces in gray correspond to regions of interest outside the displayed part of the field. The black trace represents the average. Ratio images correspond to the time points indicated by the horizontal axis. Drugs were applied in the bath for the duration indicated by the horizontal bars. The graph on the right shows the normalized average ratio change for all the regions of interest in this experiment. Time 0 was the time of the UV flash; amplitude 0 is the average of the 10 data points that precede the UV flash; amplitude was normalized to the maximal ratio change (fsk + IBMX). (C) Same as (B), except that 10 μM Lu AF64196 was applied before and during NMDA uncaging. (D) Similar experiments were averaged, with shading indicating SEM. Top: Response to NMDA uncaging measured in D1 neurons in control condition (green: n = 28, N = 4) and in the presence of 10 μM Lu AF64196 (red: n = 27, N = 5). Bottom: Response to NMDA uncaging measured in D2 neurons in control condition (green: n = 13, N = 4) and in the presence of 10 μM Lu AF64196 (red: n = 16, N = 5).

cGMP concentration of approximately 2.5 μM in a range from 1.7 to 4.0 μM.

Finally, we also monitored the calcium signal after NMDA uncaging using the genetically encoded FRET biosensor Twitch-

2B (Thestrup et al. 2014): MNI-NMDA (100 μM) uncaging was immediately followed by a large ratio increase, which declined progressively (Fig. 2D, bottom trace), over a time-course that roughly matched the transient decrease in cGMP levels.

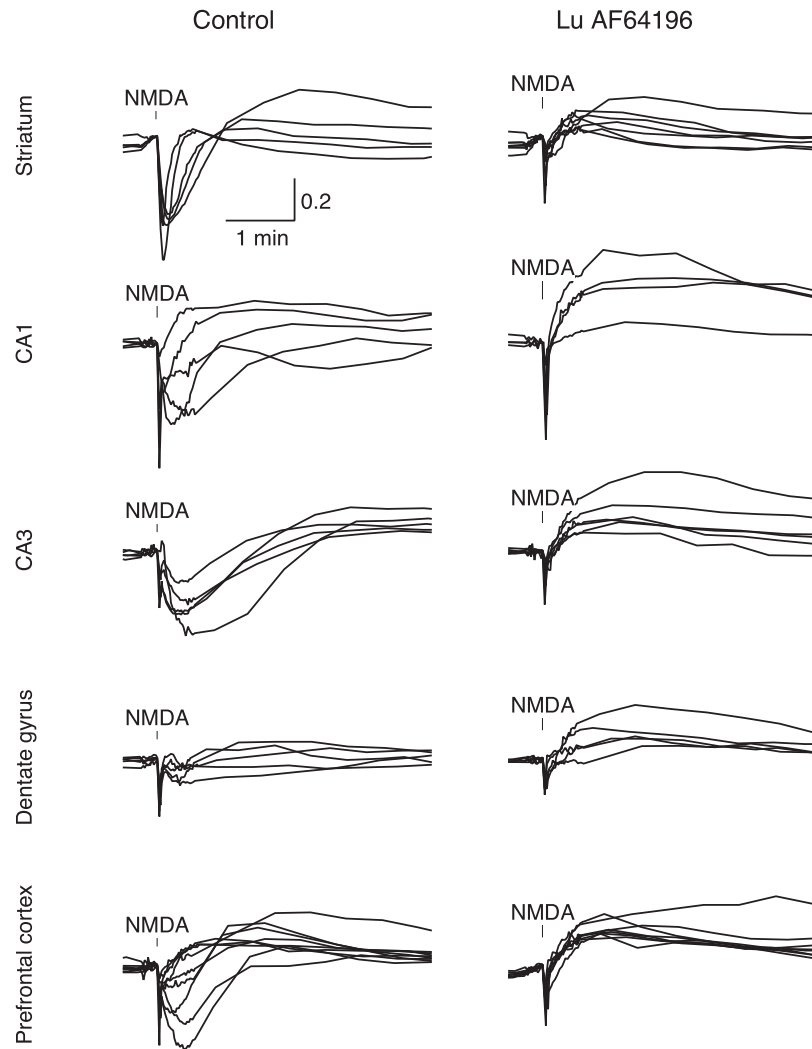


Figure 4. PDE1 effect on cGMP in various regions in mouse brain slices. NMDA was uncaged while monitoring cGMP with the cyGfAL biosensor, using the protocol shown in Figure 2. The experiment was performed in the absence (left column) or in the presence of 10 μ M Lu AF64196 (right column). Each trace represents the average ratio of one experiment comprising 1–13 neurones. Traces are normalized between baseline and maximal response to DEANO (10 μ M) and IBMX (200 μ M). The vertical bar indicates the uncaging of NMDA (100 μ M). The experiments were performed in striatum (same data as in Fig. 2), hippocampus (CA1 and CA3), dentate gyrus and prefrontal cortex. Calibration bars: horizontally, 1 min; vertically: 20% of the maximal ratio change.

These data show that a transient stimulation of NMDA receptors, which increases intracellular calcium, triggers a decrease in cGMP mediated by PDE1 action in striatal MSNs. In addition, these data show that PDE1 does not contribute significantly to cGMP control in these neurones in basal condition.

NMDA Uncaging Transiently Decreases cAMP in the Striatum

PDE1 can also hydrolyze cAMP, and to test if PDE1 controlled cAMP responses similarly to cGMP, we used the Epac-S^{H150} biosensor to monitor cAMP in striatal neurones (Fig. 3). We used a protocol for NMDA uncaging similar to that used for monitoring cGMP, except that a steady-state cAMP level was obtained with the application of 500 nM of forskolin (low fsk). MSNs were sorted in 2 groups, D1 or D2 MSNs, according to their positive cAMP response to either a D₁ agonist (SKF-81297, 100 nM) or an A_{2A} agonist (CGS 21680, 1 μ M), (Fig. 3A,B) as published previously (Yapo et al. 2017; Nair et al. 2018). At the end of the recording, the nonselective PDE inhibitor IBMX (200 μ M) was added to reach the maximal ratio response of the biosensor,

and that level was used for normalization. PDE8B is not inhibited by IBMX but its expression level is low in the brain. In addition, PDE8 has a low K_m and moderate V_{max} for cAMP compared with the highly expressed PDE2A (Rybalkin et al. 2013), and therefore PDE8 is unlikely to prevent reaching the saturation level of the biosensor. Similar to the cGMP responses, NMDA release triggered a transient decrease in cAMP in both D1 and D2 MSNs (Fig. 3B). This decrease was $-28.1 \pm 8.0\%$ (mean \pm SD, $N = 4$, $n = 28$) of the maximal ratio response in D1 MSNs, and of $-30.7 \pm 8.7\%$ (mean \pm SD, $N = 4$, $n = 13$) of the maximal ratio response in D2 MSNs, not significantly different between D1 and D2 MSNs. The recovery of the NMDA response appeared faster in D2 than in D1 MSNs, but this may be related to higher cAMP level reached in the former upon forskolin stimulation.

Similarly to cGMP, PDE1 inhibition with Lu AF64196 (10 μ M) had no effect when added to forskolin-induced cAMP steady-state level, showing a lack of PDE1 activity in the absence of a calcium signal (Fig. 3C). However, Lu AF64196 completely suppressed the transient decrease in cAMP triggered by NMDA: the decrease in cAMP level was of $-4.4 \pm 3.3\%$ (mean \pm SD, $N = 5$,

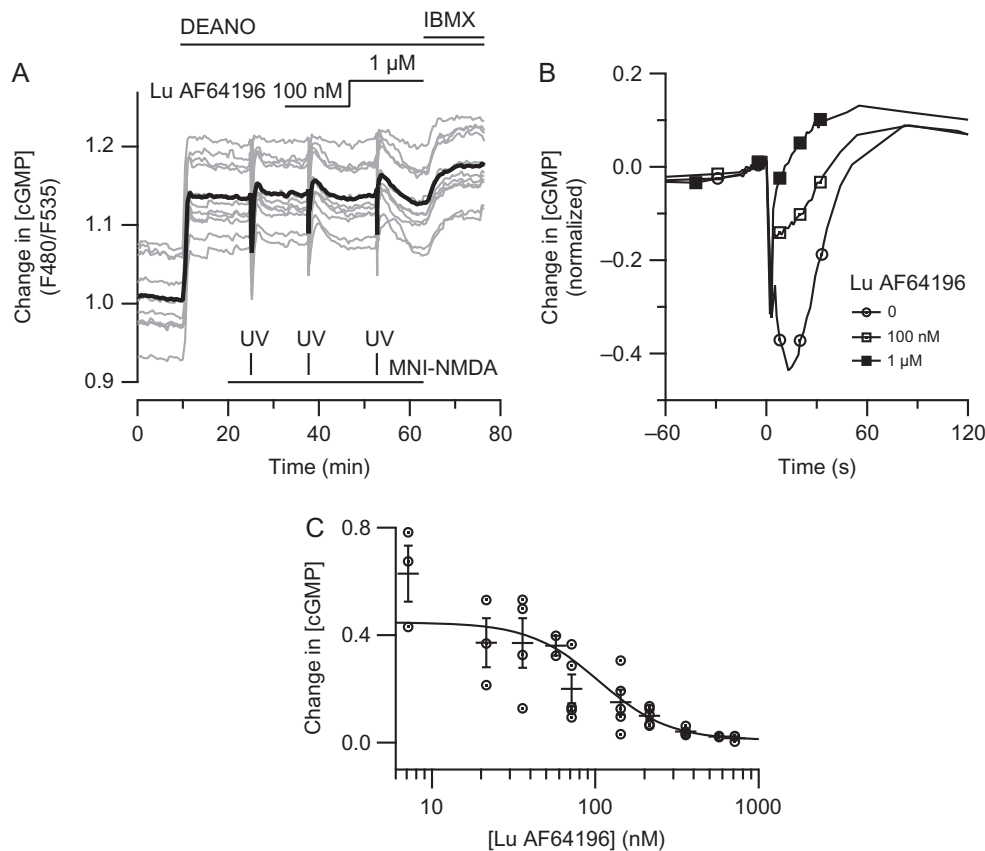


Figure 5. Dose-dependency of Lu AF64196 effect on striatal PDE1 activity in cGMP regulation. The cGMP biosensor cyGNAL was expressed in mouse striatal slices. (A) Protocol example: after elevating cGMP level with DEANO (10 μ M), 3 successive NMDA uncaging were performed. The first and third were used for normalization and were carried out at 0 and 1 μ M AF64196, respectively. The Lu AF64196 test dose was applied during the second NMDA uncaging. (B) Means of the 3 responses are overlaid for comparison. (C) Dose–response curve of the inhibitory effect of AF64196. The protocol was performed as shown in (A), testing different doses. Only one dose was tested per brain slice, represented by a circle on the plot. These data were fitted to a Hill equation with IC_{50} of 105 ± 19 nM and a Hill coefficient of 2 ± 0.6 .

$n = 27$) of the maximal ratio response in D1 MSNs, and of $-5.9 \pm 2.8\%$ (mean \pm SD, $N = 5$, $n = 16$) of the maximal ratio response in D2 MSNs. This decrease was significantly different from that measured in the absence of Lu AF64196 ($t[3.8] = 5.5$, $P = 0.0059$ for D1 MSNs, and $t[3.5] = 5.5$, $P = 0.0078$ for D2 MSNs, Fig. 3D). In contrast to the decrease obtained in control condition, NMDA uncaging in the presence of the PDE1 inhibitor led to a large rebound increase that lasted about 1 min in both D1 and D2 MSNs, possibly resulting from the activation of calcium-dependent adenylyl cyclases (Fig. 3D).

The Epac-S^{H150} ratio steady-state level reached before the UV flash was $58.0 \pm 20.3\%$ (mean \pm SD, $N = 9$, $n = 55$) of the maximal ratio response in D1 MSNs, and of $78.7 \pm 6.2\%$ (mean \pm SD, $N = 9$, $n = 29$) of the maximal ratio response in D2 MSNs. Considering a K_d of 4.4 μ M and Hill coefficient of 0.77 (Polito et al. 2013), these ratio values correspond to cAMP concentrations of 7 μ M, in a range from 3 to 20 μ M. In D2 MSNs, this level is 25 μ M in a range from 15 to 40 μ M.

These data show that PDE1 efficiently degrades cAMP following the activation of NMDA receptors. However, like for cGMP, PDE1 shows no cAMP degradation in the absence of NMDA stimulation.

PDE1 in Other Brain Regions

Besides the high expression level of PDE1B in the striatum, PDE1 is also highly expressed in cortex and hippocampus. To assess whether PDE1 is also engaged in cyclic nucleotide regulation

outside the striatum, we explored the effect of NMDA uncaging in the prefrontal cortex and in the hippocampus (CA1, CA3 and DG) using the same protocols as for measuring cGMP with the cyGNAL biosensor in the striatum (Fig. 2). This revealed a powerful action of PDE1 on cGMP level (Fig. 4) in the CA1 and CA3 regions of the hippocampus: the release of NMDA was followed by a marked decrease in cGMP concentration, which was replaced by an increase in cGMP when PDE1 was blocked by Lu AF64196 (10 μ M). The minimal ratio amplitude was measured over a temporal window from 6 to 50 s after uncaging, and expressed as a fraction of the maximal ratio response. In CA1, the ratio decrease was $-2.5 \pm 2.2\%$ (mean \pm SD, $N = 4$, $n = 7$) in the presence of Lu AF64196 versus $-22.7 \pm 11.7\%$ (mean \pm SD, $N = 5$, $n = 11$) in control condition, statistically different ($t[4.3] = 3.7$, $P = 0.017$). In CA3, the ratio decreases was $-2.8 \pm 2.5\%$ ($N = 6$, $n = 20$) versus $-31.5 \pm 16.5\%$ ($N = 5$, $n = 18$), statistically different ($t[4.2] = 3.8$, $P = 0.017$). In the cortex, some experiments showed a large decrease in cGMP after NMDA release, whereas other experiments showed minimal decrease in cGMP. In the presence of Lu AF64196, no experiment in the cortex showed any decrease in cGMP, but all displayed a sustained rebound increase in cGMP. The ratio level in the 6–50 s time range after uncaging was also higher in the presence of Lu AF64196 than in control condition, with $-3.7 \pm 4.6\%$ ($N = 8$, $n = 36$) versus $-14.9 \pm 12.2\%$ ($N = 9$, $n = 26$; $t[10.4] = 2.5$, $P = 0.028$), showing that PDE1 can down-regulate cGMP in cortical neurones, or at least in a subset thereof. The contribution of PDE1 in the degradation of cGMP in the dentate gyrus was clearly

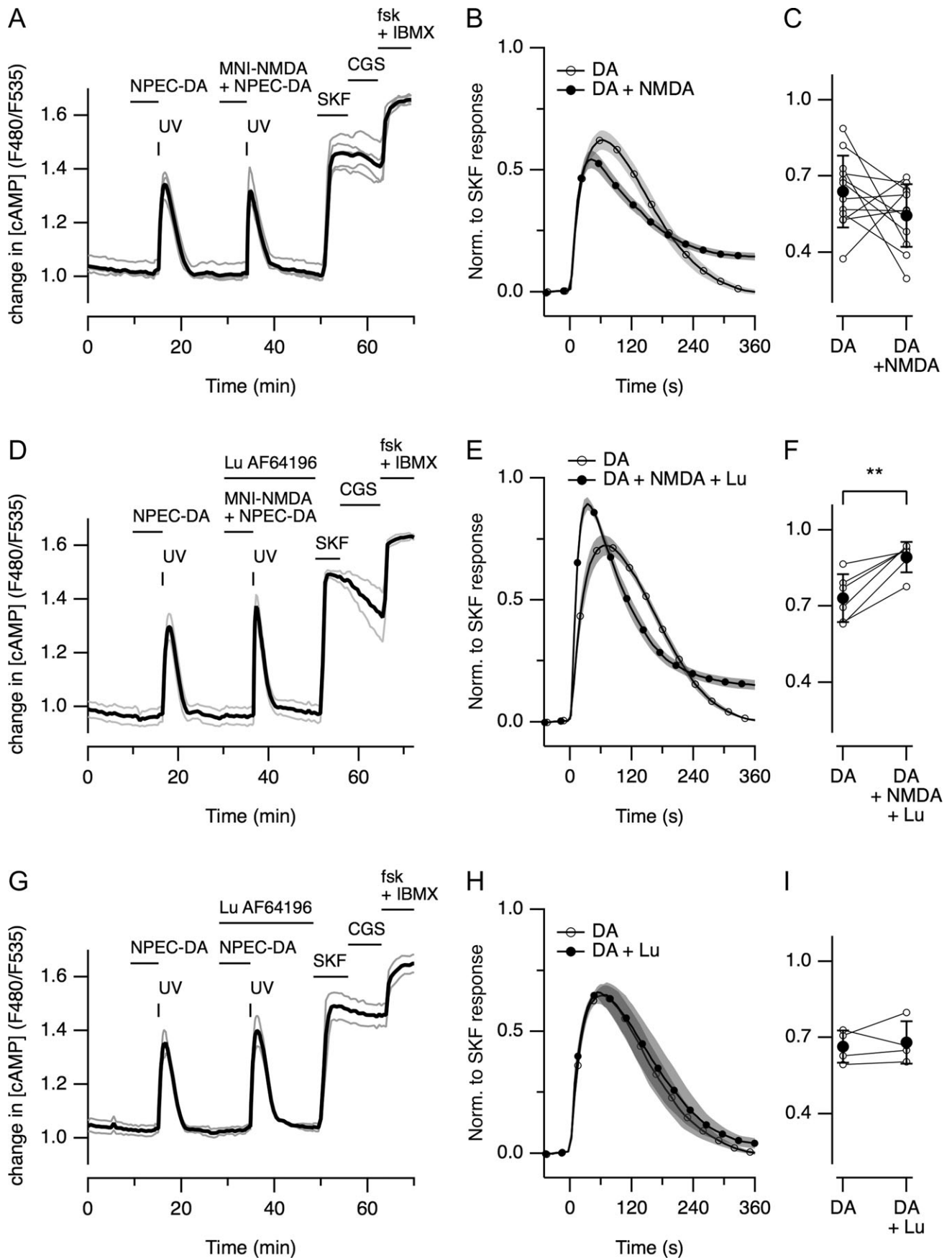


Figure 6. PDE1 opposes the potentiation of the cAMP response to dopamine induced by NMDA. Striatal brain slices from mouse expressing the Epac-S^{H150} biosensor. (A) NPEC-DA (3 μ M) was applied in the bath, and dopamine was released by a flash of UV light to trigger the control cAMP response. After recovery to baseline, a second uncaging episode was performed in the presence of both NPEC-DA (3 μ M) and MNI-NMDA (100 μ M). (B) Average of the first and second peak from 12 similar experiments. Shading indicates SEM. (C) Amplitude of the first and second cAMP peak for all experiment. Average \pm SEM is represented by the filled circle. (D–F) Same as A–C except that Lu AF64193 (1 μ M) was added during and after the second uncaging episode. (G–I) Same as A–C, except that no MNI-NMDA was applied.

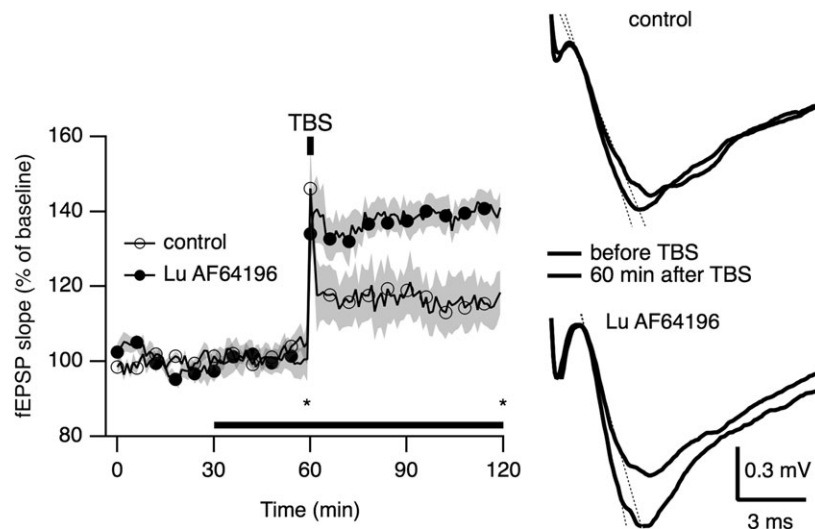


Figure 7. Lu AF64196 potentiates the LTP response. Rat brain slices were prepared from ventral striatum. Left: Normalized fEPSP slope as a function of time. Bath application of Lu AF64196 (3 μ M, $n = 8$, $N = 5$) increased the fEPSP slope following theta burst stimulation (TBS) when compared with DMSO treated (control) slices ($n = 9$, $N = 5$). Gray shading indicates SEM. The horizontal bar indicates the period during which Lu AF64196 or DMSO were added to the perfusing ACSF. TBS was applied at time 60 min: 10 bursts delivered at 200 ms interval—each burst consisting of 4 pulses at 50 Hz, repeated 10 times at 15 s intervals. Right: Traces show representative fEPSP traces before and after TBS (at times indicated by * on the left graph) in the absence (control) or in the presence of Lu AF64196. Dotted lines indicate the linear fit of response onset, which slope was used to quantify fEPSP.

visible on the shape of the ratio traces (Fig. 4), but the amplitude measured in the 6–50 s time range did not show a statistically significant difference, mainly because of the small absolute ratio changes. This is consistent with these neurons being highly hyperpolarised (Staley et al. 1992), therefore keeping NMDA receptor blocked with magnesium. To better account for decrease in cGMP concentration mediated by PDE1, the slope of the ratio trace was calculated over a 6–20 s time range. This slope, expressed as a fraction of normalized ratio per second was $+5.38 \pm 3.3\%$ (mean \pm SD, $N = 5$, $n = 22$) with Lu AF64196 versus $-2.0 \pm 2.3\%$ ($N = 5$, $n = 24$) in control condition ($t[7.1] = 4.1$, $P = 0.004$).

A similar experimental protocol was applied with the Epac-S^{H150} cAMP biosensor on the same brain regions. While the effect of Lu AF64196 was visible qualitatively, the results were more complex to analyze, with a large variability of the NMDA-induced response (Supplementary Fig. S3).

Overall, these experiments reveal a clear contribution of PDE1 in the regulation of cGMP in the striatum, hippocampus and cortex after the transient activation of NMDA receptors. An effect of PDE1 on cAMP was also clear in the striatum, but more refined protocols are required to quantify its role on cAMP in other brain regions.

Dose-Response Analysis in the Striatum With cGMP

To determine the dose-dependency of the Lu AF64196 effect on PDE1 activity in mouse brain slice preparations, we focused on its action on cGMP in the striatum. Since the amplitude of the PDE1-mediated decrease in cGMP varied from cell to cell, the effect of each dose of Lu AF64196 was quantified using 3 successive NMDA uncaging episodes (Fig. 5): an initial control uncaging was performed without Lu AF64196, a second uncaging was done in the presence of Lu AF64196 at the test concentration and a third uncaging was performed in the presence of a maximal dose of Lu AF64196 (1 μ M). We verified that 3 consecutive episodes of NMDA uncaging produced similar decreases in cGMP (Supplementary Fig. S4A), and that 1 μ M Lu AF64196 was sufficient to completely block the decrease in cGMP (Supplementary Fig. S4B). The effect of the Lu AF64196 test

concentration (second uncaging event) was normalized to the uncaging events with no and maximal (1 μ M) Lu AF64196 (Fig. 5A,B). This protocol was repeated for Lu AF64196 doses ranging from 7 to 730 nM in the striatum. A single dose was tested in each experiment. The peak amplitude of the cGMP response to NMDA were averaged for each experiment, and provided a dose-response curves which was fitted to a Hill equation with IC₅₀ of 105 nM (Fig. 5C).

Dopamine—NMDA Coincidence in the Striatum

Coincidence of dopamine and glutamate neurotransmission is considered to be a key mechanism underlying learning processes in the striatum (Surmeier et al. 2007; Kreitzer & Malenka 2008; Cerovic et al. 2013), and we wanted to determine whether the cAMP signal produced by dopamine D₁-like receptors in the striatum are affected by PDE1 activity triggered by the concomitant release of NMDA. To this end, we used NPEC-dopamine (NPEC-DA, “caged dopamine”), which has previously been shown to consistently induce large increases in cAMP in D1 MSNs (Yapo et al. 2017). Experiments were performed on mouse striatal slices expressing the cAMP biosensor Epac-S^{H150} (Fig. 6A). These experiments were performed with TTX (200 nM), atropine (1 μ M), CGP 55845A (100 nM), AM251 (100 nM), naloxone (500 nM) and eticlopride (100 nM) to block voltage-dependent sodium channels, muscarinic, GABA_B, CB₁, opioid, and dopamine D₂-like receptors, respectively. D1 and D2 MSNs were identified at the end of the experiment from their response to either D₁ or A_{2A} receptor agonists SKF-81297 (100 nM) or CGS 21680 (1 μ M), respectively (Yapo et al. 2017) and as illustrated in Figure 3A, and only D1 MSNs were analyzed. A first reference dopamine response was measured with the uncaging of NPEC-DA (3 μ M); a second response was measured with the simultaneous uncaging of NPEC-DA (3 μ M) and MNI-NMDA (100 μ M). The same experiment was repeated and Figure 6B shows the average of the first and second peaks. The recovery kinetics appeared somewhat slower on the second peak. The amplitude of the cAMP responses were similar ($64 \pm 4\%$ of the response to SKF for the first peak vs. $54 \pm 4\%$, mean \pm SEM for the

second peak, $N = 12$, $n = 59$, not significantly different) ($t[11]=1.5$, $P=0.15$; peak amplitudes are shown in Fig. 7C).

To test the involvement of PDE1 in the regulation of the dopamine-induced cAMP peak, a second set of similar experiments was performed in which Lu AF64196 (1 μM) was applied a few minutes before and maintained during and after the co-release of dopamine and NMDA (Fig. 6D). In contrast to the control condition, the amplitude of the cAMP response produced by co-release of NMDA and dopamine was increased when PDE1 was inhibited (Fig. 6E,F): the amplitude of the first peak was $73 \pm 4\%$ versus $89 \pm 2\%$, $N = 6$, $n = 23$ for the second peak, significantly different (paired t -test, $t[5] = 5.2$, $P = 0.003$). As a control, we verified that Lu AF64196 had no effect on the dopamine response in the absence of NMDA (Fig. 6G–I, paired t -test, $t[3] = 0.51$, $P = 0.65$).

These experiments show that PDE1 modulates the amplitude of a dopamine-induced cAMP signal in the context of coincidental activation of NMDA and D_1 receptors.

PDE1 Action in Synaptic Plasticity

The cAMP/PKA signaling pathway, activated by D_1 receptors in $D1$ MSNs and adenosine A_{2A} receptors in $D2$ MSNs, is required for LTP induction (Kreitzer & Malenka 2008; Surmeier et al. 2009; Cerovic et al. 2013), and since we observed that PDE1 opposed the dopamine-induced cAMP signal, we wondered whether PDE1 action might reduce LTP induction. The effect of Lu AF64196 (3 μM) on LTP in the ventral striatum (NAc) was tested using field recordings in rat brain slices (Fig. 7). To isolate the response to glutamatergic synapses, GABA_A receptor activity was blocked by supplying Gabazine (10 μM) to the perfusing ACSF. Slices were subjected to Lu AF64196 or DMSO for 30 min prior to theta-burst stimulation (TBS) and during this period fEPSP slopes remained largely unaffected by the presence of compound, indicating that basal cAMP/cGMP levels and/or intracellular Ca^{2+} concentration are too low to observe an effect of PDE1 activity under these conditions. TBS induced an increase in the fEPSP slope, which remained elevated during the time course of the experiment, both in the absence and the presence of Lu AF64196 (3 μM). Lu AF64196 increased the average fEPSP slope 50–60 min after TBS to $140 \pm 4.5\%$ (mean \pm SEM, $N = 5$, $n = 8$) relative to prestimulation levels, which is significantly higher than in DMSO controls ($113 \pm 5.4\%$, mean \pm SEM, $N = 5$, $n = 9$, $t(15) = 3.785$, $P = 0.002$). Thus, PDE1 inhibition results in an increased LTP response in NAc, consistent with PDE1 opposing the cAMP signals which are required for LTP induction.

Discussion

PDE1 is highly expressed in the brain, but there are little mechanistic data on its functional impact in neurons. Using the selective PDE1 inhibitor Lu AF64196 and biosensors for cyclic nucleotides, we describe PDE1 action on both cAMP and cGMP in mouse brain slice preparations. Our experiments reveal that, upon activation of NMDA receptors, PDE1 degrades cAMP and cGMP in the striatum, cortex, and hippocampus. Our results also show that PDE1 is implicated in the regulation of synaptic plasticity, and that it regulates the effect of dopamine when NMDA receptors are stimulated at the same time.

While the palette of biosensors for cAMP now includes bright sensors with high signal change (Polito et al. 2013; Klarenbeek et al. 2011, 2015), biosensors for cGMP with similarly high ratio changes and good photostability have been missing. From the first cygnet family of biosensors for cGMP developed by W. Dostman (Honda et al. 2001, 2005), a number of more recent sensors were created with various cGMP sensing

domains and architecture, like cGES-DE5 (Nikolaev et al. 2006) or the cGi series (Russwurm et al. 2007). All these cGMP biosensors are discussed in detail in a recent review (Russwurm & Koesling 2018). Since PDE1 can hydrolyze both cAMP and cGMP, it was critical that our biosensors had a high selectivity for each cyclic nucleotide. The Epac-S^{H150} biosensor has already been reported to be unresponsive to the high cGMP levels obtained in striatal neurons by application of NO donors (Polito et al. 2013). The cyGNAL biosensor developed here showed a high selectivity for cGMP against cAMP. With a K_d of 465 nM for cGMP, high selectivity against cAMP, a large ratio change and bright fluorophores, this biosensor proved suitable for measuring cGMP in brain slice preparations.

Increased intracellular calcium—and in particular through the activation of NMDA receptors—can stimulate the synthesis of cyclic nucleotides through various mechanisms. This effect can be direct, for example via the calcium-activated adenylyl cyclase AC1 and AC8. In addition, the activation of local neurons can lead to the release of neuromodulatory compounds such as NO (Garthwaite 2019). In the cortex, we have already shown that VIP, CRF and PACAP can trigger powerful cAMP signals (Hu et al. 2011), and NMDA stimulation may release such neuropeptides locally. How PDE1 could oppose such changes in cyclic nucleotide signal has been so far difficult to characterize, for lack of measurement methods with sufficient sensitivity and temporal resolution. Using biosensor imaging, we first tested whether PDE1 could revert an artificially induced high steady-state level of cyclic nucleotide, in conditions of action potential inhibition. Transient activation of NMDA receptors efficiently decreased both cGMP and cAMP levels, effects that were blocked by the PDE1 inhibitor Lu AF64196, and therefore attributable to PDE1 action. The transient decrease roughly matched the kinetics of the increase in intracellular calcium, on the time-scale of a minute. Such transient decrease was observed in all the brain regions that were included in our studies in which PDE1A and/or PDE1B are expressed (although it was not present in all neurons in the prefrontal cortex). Interestingly, full PDE1 inhibition revealed an increase in cyclic nucleotide level that follows the calcium signal, although on a slightly slower time-scale. The precise mechanisms underlying these increases remain to be identified and may involve calcium-induced activation of adenylyl cyclases AC1 or AC8 in the case of cAMP, and an increase in NO concentration resulting from NMDA-dependent activation of nNOS. TTX may also be insufficient to prevent the release of endogenous neuropeptides. PDE1 action thus opposes the NMDA-induced increase in cyclic nucleotide levels. While these 2 opposite effects may seem physiologically inconsistent, it potentially opens for a richer array of integrative properties. Indeed, further work is needed to determine the precise spatial and temporal features of these cyclic nucleotide events at the level of single synapses where it determines plasticity.

In striatal MSNs where PDE1B is highly expressed, we observed that the application of Lu AF64196 alone had no effect on cyclic nucleotide levels showing that PDE1 has no functional activity in the absence of a calcium signal (Figs 2C and 3C). This is consistent with a tight control of calcium-calmodulin in living neurons, sufficient to maintain PDE1 activity below our detection threshold. This contrasts with striatal PDE2A which, although activated by cGMP, displays a clear activity even in the absence of elevated cGMP (Polito et al. 2013). Among the regulated PDEs, PDE1 thus appears to strictly require calcium to operate, which suggests a tight link between PDE1 function and neuronal activity or excitatory synaptic input.

Our experiments in the striatum show that PDE1 efficiently degrades both cAMP and cGMP. PDEs have different K_m values for cyclic nucleotides which determines the concentration of cyclic nucleotide onto which it operates (Neves-Zaph 2017): in cells expressing a combination of PDEs, cyclic nucleotide signals in different concentration ranges are controlled by different PDEs. This has been illustrated in HEK293 cells in which PDE3 and PDE10A control cAMP signals elicited by minimal stimulation, whereas PDE4 action is only visible for more powerful stimulations (Matthiesen & Nielsen 2011). The high K_m value of PDE1B for cGMP and cAMP (5 and 33 μM , respectively) (Poppe et al. 2008) suggests that PDE1 would be efficient on high concentrations of cyclic nucleotides. Indeed, in MSNs, the steady-state cyclic nucleotide levels before NMDA uncaging (around 2 μM cGMP and 7–25 μM cAMP) at which a consistent PDE1-mediated response was observed, were in the same order of magnitude as the respective K_m of PDE1B. Biosensor imaging has already shown that cAMP levels could rise to particularly high level in the striatum compared with the cortex (Castro et al. 2013), which could explain why PDE1 exerted such powerful effect in MSNs. In contrast, the lower cAMP level reached in the cortex may in part explain why the action of PDE1 was observed less consistently in this brain region. Indeed, PDE4 has already been shown to be critical in controlling large cAMP signals in this part of the brain (Castro et al. 2010; Kuroiwa et al. 2012), and PDE4 action may be masking a comparatively smaller PDE1 contribution. However, other factors such as differences in PDE1 expression in a brain region with higher neuronal diversity are also likely to contribute.

PDE2A and PDE10A are also dual specificity enzymes, and constitute with PDE1B the major PDE types expressed in MSNs. PDE2A also displays a high K_m for cGMP and cAMP (31 and 112 μM , respectively) (Poppe et al. 2008), and PDE2A was also shown to degrade high cAMP and cGMP levels (Polito et al. 2013). This suggests that PDE1B and PDE2A simultaneously regulate high cyclic nucleotide levels in MSNs. However, their action differ in the ways they are regulated, with PDE1B strictly depending on glutamatergic inputs, and PDE2A being activated by NOergic interneurons, but also having a notable activity in the absence of cGMP (Polito et al. 2013). In contrast, PDE10A shows no or modest regulation by cAMP (Matthiesen & Nielsen 2009; Jager et al. 2012), has a high affinity for cAMP (K_m of 0.67 μM) (Poppe et al. 2008), and was shown to regulate the sub-micromolar cAMP level resulting from basal cAMP production (Polito et al. 2015). In summary, our experiments clarify the functional conditions in which PDE1B operates in the striatum: dual specificity, performing on high cyclic nucleotide levels and requiring a calcium signal such as that triggered by glutamatergic inputs.

Both cAMP and cGMP play important roles in synaptic plasticity and transmission in general (Kandel 2001; Garthwaite 2008) and particularly in the striatum (Lovinger 2010; Threlfell & West 2013; Padovan-Neto & West 2017). In the case of cGMP, in vivo studies have demonstrated the importance of NO production by interneurons, which control both the excitability of MSNs and the efficacy of cortico-striatal synaptic transmission (Padovan-Neto et al. 2015), while in addition, cGMP and calcium induce LTD (Calabresi et al. 1999). In parallel, direct glutamatergic inputs from the cortex increase calcium in MSNs, which activates PDE1B and opposes the NO-induced increase in cGMP. The efficacy of cortico-striatal synaptic transmission will thus result from a complex balance between these effects, and more experimental work is required to determine the contribution of PDE1B in the various schemes of synaptic regulation. In the case of cAMP, dopamine through D_1 receptors has been shown

to play a critical role in reward-mediated learning in the striatum, and LTP induction requires the activation of D_1 receptors (Kreitzer & Malenka 2008; Surmeier et al. 2009; Lovinger 2010; Cerovic et al. 2013). We report here that the positive cAMP response elicited by D_1 receptors is reduced by the co-activation of NMDA receptors. This is consistent with the observed potentiation of LTP upon PDE1 inhibition, in which PDE1 opposes the rise in cAMP which is needed for synaptic plasticity.

Collectively, these observations highlight PDE1 as a negative regulator of cyclic nucleotide signaling operating at the cross-road between calcium and cyclic nucleotide signaling pathways, and therefore endowed with a critical function in fine-tuning synaptic plasticity. By showing that PDE1 is involved in the coincidence detection of glutamate-mediated calcium signals with dopamine or NO signals, our study strongly supports that PDE1 inhibitors could have a therapeutic value, in particular in conditions related to hypodopaminergia.

Supplementary Material

Supplementary material is available at *Cerebral Cortex* online.

Funding

Lundbeck A/S and by the “Investissements d’Avenir” program managed by the ANR under reference ANR-11-IDEX-0004-02.

Note

We would like to thank Drs Régis Blaise and Jean-Christophe Poncer for helpful comments on the article. O.G. and P.V. received a funding for cooperation from “Bayerisch-Französisches Hochschulzentrum.” O.G. was an invited scientist of Ecole des Neurosciences de Paris. The group of E.M., P.V., and L.R.V.C. is member of the Bio-Psy Labex. *Conflicts of interests:* J.N., C.H., C.T.C., and J.K. are employed by H. Lundbeck A/S. J.Y. has worked as a consultant for the company H. Lundbeck A/S. The PDE1 inhibitor used in this study has been generated by Lundbeck.

References

- Ahmad F, Murata T, Shimizu K, Degerman E, Maurice D, Manganiello V. 2015. Cyclic nucleotide phosphodiesterases: important signaling modulators and therapeutic targets. *Oral Dis.* 21:e25–e50.
- Ahn HS, Crim W, Romano M, Sybertz E, Pitts B. 1989. Effects of selective inhibitors on cyclic nucleotide phosphodiesterases of rabbit aorta. *Biochem Pharmacol.* 38:3331–3339.
- Bertran-Gonzalez J, Hervé D, Girault JA, Valjent E. 2010. What is the degree of segregation between striatonigral and striatopallidal projections. *Front Neuroanat.* 4:136.
- Calabresi P, Gubellini P, Centonze D, Sancesario G, Morello M, Giorgi M, Pisani A, Bernardi G. 1999. A critical role of the nitric oxide/cGMP pathway in corticostriatal long-term depression. *J Neurosci.* 19:2489–2499.
- Castro LR, Brito M, Guiot E, Polito M, Korn CW, Herve D, Girault JA, Paupardin-Tritsch D, Vincent P. 2013. Striatal neurones have a specific ability to respond to phasic dopamine release. *J Physiol.* 591:3197–3214.
- Castro LR, Gervasi N, Guiot E, Cavellini L, Nikolaev VO, Paupardin-Tritsch D, Vincent P. 2010. Type 4 phosphodiesterase plays different integrating roles in different cellular domains in pyramidal cortical neurons. *J Neurosci.* 30:6143–6151.

- Cerovic M, d'Isa R, Tonini R, Brambilla R. 2013. Molecular and cellular mechanisms of dopamine-mediated behavioral plasticity in the striatum. *Neurobiol Learn Mem.* 105:63–80.
- Dorner-Ciossek C, Kroker KS, Rosenbrock H. 2017. Role of PDE9 in cognition. *Adv Neurobiol.* 17:231–254.
- Ehrenguber MU, Lundstrom K, Schweitzer C, Heuss C, Schlesinger S, Gähwiler BH. 1999. Recombinant Semliki Forest virus and Sindbis virus efficiently infect neurons in hippocampal slice cultures. *Proc Natl Acad Sci U S A.* 96:7041–7046.
- Ehrman LA, Williams MT, Schaefer TL, Gudelsky GA, Reed TM, Fienberg AA, Greengard P, Vorhees CV. 2006. Phosphodiesterase 1B differentially modulates the effects of methamphetamine on locomotor activity and spatial learning through DARPP32-dependent pathways: evidence from PDE1B-DARPP32 double-knockout mice. *Genes Brain Behav.* 5:540–551.
- Fabritius A, Ng D, Kist AM, Erdogan M, Portugues R, Griesbeck O. 2018. Imaging-based screening platform assists protein engineering. *Cell Chem Biol.* 25:1554–1561.e8.
- Garthwaite J. 2008. Concepts of neural nitric oxide-mediated transmission. *Eur J Neurosci.* 27:2783–2802.
- Garthwaite J. 2019. NO as a multimodal transmitter in the brain: discovery and current status. *Br J Pharmacol.* 176:197–211.
- Giorgi M, D'Angelo V, Esposito Z, Nuccetelli V, Sorge R, Martorana A, Stefani A, Bernardi G, Sancesario G. 2008. Lowered cAMP and cGMP signalling in the brain during levodopa-induced dyskinesias in hemiparkinsonian rats: new aspects in the pathogenetic mechanisms. *Eur J Neurosci.* 28:941–950.
- Goraya TA, Cooper DM. 2005. Ca²⁺-calmodulin-dependent phosphodiesterase (PDE1): current perspectives. *Cell Signal.* 17:789–797.
- Hansen RS, Beavo JA. 1986. Differential recognition of calmodulin-enzyme complexes by a conformation-specific anti-calmodulin monoclonal antibody. *J Biol Chem.* 261:14636–14645.
- Hawes SL, Gillani F, Evans RC, Benkert EA, Blackwell KT. 2013. Sensitivity to theta-burst timing permits LTP in dorsal striatal adult brain slice. *J Neurophysiol.* 110:2027–2036.
- Honda A, Adams SR, Sawyer CL, Lev-Ram V, Tsien RY, Dostmann WRG. 2001. Spatiotemporal dynamics of guanosine 3',5'-cyclic monophosphate revealed by a genetically encoded, fluorescent indicator. *Proc Natl Acad Sci USA.* 98:2437–2442.
- Honda A, Sawyer CL, Cawley SM, Dostmann WR. 2005. Cygnets: in vivo characterization of novel cGMP indicators and in vivo imaging of intracellular cGMP. *Methods Mol Biol.* 307:27–43.
- Hu E, Demmou L, Cauli B, Gallopin T, Geoffroy H, Harris-Warrick RM, Paupardin-Tritsch D, Lambollez B, Vincent P, Hepp R. 2011. VIP, CRF, and PACAP act at distinct receptors to elicit different cAMP/PKA dynamics in the neocortex. *Cereb Cortex.* 21:708–718.
- Huang GY, Kim JJ, Reger AS, Lorenz R, Moon EW, Zhao C, Casteel DE, Bertinetti D, Vanschouwen B, Selvaratnam R, et al. 2014. Structural basis for cyclic-nucleotide selectivity and cGMP-selective activation of PKG I. *Structure.* 22:116–124.
- Jager R, Russwurm C, Schwede F, Genieser HG, Koesling D, Russwurm M. 2012. Activation of PDE10 and PDE11 phosphodiesterases. *J Biol Chem.* 287:1210–1219.
- Kandel ER. 2001. The molecular biology of memory storage: a dialogue between genes and synapses. *Science.* 294:1030–1038.
- Kelly MP, Adamowicz W, Bove S, Hartman AJ, Mariga A, Pathak G, Reinhart V, Romegialli A, Kleiman RJ. 2014. Select 3',5'-cyclic nucleotide phosphodiesterases exhibit altered expression in the aged rodent brain. *Cell Signal.* 26:383–397.
- Keravis T, Lugnier C. 2012. Cyclic nucleotide phosphodiesterase (PDE) isozymes as targets of the intracellular signalling network: benefits of PDE inhibitors in various diseases and perspectives for future therapeutic developments. *Br J Pharmacol.* 165:1288–1305.
- Khammy MM, Dalsgaard T, Larsen PH, Christoffersen CT, Clausen D, Rasmussen LK, Folkersen L, Grunnet M, Kehler J, Aalkjaer C, et al. 2017. PDE1A inhibition elicits cGMP-dependent relaxation of rat mesenteric arteries. *Br J Pharmacol.* 174:4186–4198.
- Kim JJ, Casteel DE, Huang G, Kwon TH, Ren RK, Zwart P, Headd JJ, Brown NG, Chow DC, Palzkill T, et al. 2011. Co-crystal structures of PKG I β (92–227) with cGMP and cAMP reveal the molecular details of cyclic-nucleotide binding. *PLoS One.* 6:e18413.
- Klarenbeek JB, Goedhart J, Hink MA, Gadella TW, Jalink K. 2011. A mTurquoise-based cAMP sensor for both FLIM and ratio-metric read-out has improved dynamic range. *PLoS One.* 6:e19170.
- Klarenbeek J, Goedhart J, van Batenburg A, Groenewald D, Jalink K. 2015. Fourth-generation Epac-based FRET sensors for cAMP feature exceptional brightness, photostability and dynamic range: characterization of dedicated sensors for FLIM, for ratiometry and with high affinity. *PLoS One.* 10:e0122513.
- Kreitzer AC, Malenka RC. 2008. Striatal plasticity and basal ganglia circuit function. *Neuron.* 60:543–554.
- Kuroiwa M, Snyder GL, Shuto T, Fukuda A, Yanagawa Y, Benavides DR, Nairn AC, Bibb JA, Greengard P, Nishi A. 2012. Phosphodiesterase 4 inhibition enhances the dopamine D1 receptor/PKA/DARPP-32 signaling cascade in frontal cortex. *Psychopharmacology (Berl).* 219:1065–1079.
- Lakics V, Karran EH, Boess FG. 2010. Quantitative comparison of phosphodiesterase mRNA distribution in human brain and peripheral tissues. *Neuropharmacology.* 59:367–374.
- Lovinger DM. 2010. Neurotransmitter roles in synaptic modulation, plasticity and learning in the dorsal striatum. *Neuropharmacology.* 58:951–961.
- Lugnier C. 2006. Cyclic nucleotide phosphodiesterase (PDE) superfamily: a new target for the development of specific therapeutic agents. *Pharmacol Ther.* 109:366–398.
- Lugnier C, Schoeffter P, Le Bec A, Strouthou E, Stoclet JC. 1986. Selective inhibition of cyclic nucleotide phosphodiesterases of human, bovine and rat aorta. *Biochem Pharmacol.* 35:1743–1751.
- Markwardt ML, Kremers GJ, Kraft CA, Ray K, Cranfill PJ, Wilson KA, Day RN, Wachter RM, Davidson MW, Rizzo MA. 2011. An improved cerulean fluorescent protein with enhanced brightness and reduced reversible photoswitching. *PLoS One.* 6:e17896.
- Matthiesen K, Nielsen J. 2009. Binding of cyclic nucleotides to phosphodiesterase 10 A and 11 A GAF domains does not stimulate catalytic activity. *Biochem J.* 423:401–409.
- Matthiesen K, Nielsen J. 2011. Cyclic AMP control measured in two compartments in HEK293 cells: phosphodiesterase K(M) is more important than phosphodiesterase localization. *PLoS One.* 6:e24392.
- Maurice DH, Ke H, Ahmad F, Wang Y, Chung J, Manganiello VC. 2014. Advances in targeting cyclic nucleotide phosphodiesterases. *Nat Rev Drug Discov.* 13:290–314.
- Medina AE. 2011. Therapeutic utility of phosphodiesterase type I inhibitors in neurological conditions. *Front Neurosci.* 5:21.
- Menniti FS, Faraci WS, Schmidt CJ. 2006. Phosphodiesterases in the CNS: targets for drug development. *Nat Rev Drug Discov.* 5:660–670.
- Nair AG, Castro LRV, El Khoury M, Gorgievski V, Giros B, Tzavara ET, Hellgren-Kotaleski J, Vincent P. 2018. The high efficacy of muscarinic M4 receptor in D1 medium spiny neurons reverses striatal hyperdopaminergia. *Neuropharmacology.* 146:74–83.

- Neves-Zaph SR. 2017. Phosphodiesterase diversity and signal processing within cAMP signaling networks. *Adv Neurobiol.* 17:3–14.
- Nguyen AW, Daugherty PS. 2005. Evolutionary optimization of fluorescent proteins for intracellular FRET. *Nat Biotechnol.* 23:355–360.
- Nikolaev VO, Gambaryan S, Lohse MJ. 2006. Fluorescent sensors for rapid monitoring of intracellular cGMP. *Nat Methods.* 3:23–25.
- Padovan-Neto FE, Sammut S, Chakroborty S, Dec AM, Threlfell S, Campbell PW, Mudrakola V, Harms JF, Schmidt CJ, West AR. 2015. Facilitation of corticostriatal transmission following pharmacological inhibition of striatal phosphodiesterase 10 A: role of nitric oxide-soluble guanylyl cyclase-cGMP signaling pathways. *J Neurosci.* 35:5781–5791.
- Padovan-Neto FE, West AR. 2017. Regulation of striatal neuron activity by cyclic nucleotide signaling and phosphodiesterase inhibition: implications for the treatment of Parkinson's disease. *Adv Neurobiol.* 17:257–283.
- Pekcec A, Schülert N, Stierstorfer B, Deiana S, Dorner-Ciossek C, Rosenbrock H. 2018. Targeting the dopamine D₁ receptor or its downstream signalling by inhibiting phosphodiesterase-1 improves cognitive performance. *Br J Pharmacol.* 175:3021–3033.
- Piedrafita B, Cauli O, Montoliu C, Felipo V. 2007. The function of the glutamate-nitric oxide-cGMP pathway in brain in vivo and learning ability decrease in parallel in mature compared with young rats. *Learn Mem.* 14:254–258.
- Polito M, Guiot E, Gangarossa G, Longueville S, Doulazmi M, Valjent E, Hervé D, Girault JA, Paupardin-Tritsch D, Castro LR, et al. 2015. Selective effects of PDE10A inhibitors on striatopallidal neurons require phosphatase inhibition by DARPP-32. *eNeuro.* 2:1–15.
- Polito M, Klarenbeek J, Jalink K, Paupardin-Tritsch D, Vincent P, Castro LR. 2013. The NO/cGMP pathway inhibits transient cAMP signals through the activation of PDE2 in striatal neurons. *Front Cell Neurosci.* 7:211.
- Polli JW, Kincaid RL. 1994. Expression of a calmodulin-dependent phosphodiesterase isoform (PDE1B1) correlates with brain regions having extensive dopaminergic innervation. *J Neurosci.* 14:1251–1261.
- Poppe H, Rybalkin SD, Rehmann H, Hinds TR, Tang XB, Christensen AE, Schwede F, Genieser HG, Bos JL, Doskeland SO, et al. 2008. Cyclic nucleotide analogs as probes of signaling pathways. *Nat Methods.* 5:277–278.
- Reed TM, Repaske DR, Snyder GL, Greengard P, Vorhees CV. 2002. Phosphodiesterase 1B knock-out mice exhibit exaggerated locomotor hyperactivity and DARPP-32 phosphorylation in response to dopamine agonists and display impaired spatial learning. *J Neurosci.* 22:5188–5197.
- Reneerkens OA, Rutten K, Steinbusch HW, Blokland A, Prickaerts J. 2009. Selective phosphodiesterase inhibitors: a promising target for cognition enhancement. *Psychopharmacology (Berl).* 202:419–443.
- Russwurm M, Koesling D. 2018. Measurement of cGMP-generating and -degrading activities and cGMP levels in cells and tissues: focus on FRET-based cGMP indicators. *Nitric Oxide.* 77:44–52.
- Russwurm M, Mullershausen F, Friebe A, Jager R, Russwurm C, Koesling D. 2007. Design of fluorescence resonance energy transfer (FRET)-based cGMP indicators: a systematic approach. *Biochem J.* 407:69–77.
- Rybalkin SD, Hinds TR, Beavo JA. 2013. Enzyme assays for cGMP hydrolyzing phosphodiesterases. *Methods Mol Biol.* 1020:51–62.
- Sancesario G, Giorgi M, D'Angelo V, Modica A, Martorana A, Morello M, Bengtson CP, Bernardi G. 2004. Down-regulation of nitrenergic transmission in the rat striatum after chronic nigrostriatal deafferentation. *Eur J Neurosci.* 20:989–1000.
- Sancesario G, Morrone LA, D'Angelo V, Castelli V, Ferrazzoli D, Sica F, Martorana A, Sorge R, Cavaliere F, Bernardi G, et al. 2014. Levodopa-induced dyskinesias are associated with transient down-regulation of cAMP and cGMP in the caudate-putamen of hemiparkinsonian rats: reduced synthesis or increased catabolism. *Neurochem Int.* 79:44–56.
- Schmidt CJ. 2010. Phosphodiesterase inhibitors as potential cognition enhancing agents. *Curr Top Med Chem.* 10:222–230.
- Sitges M, Galván E, Nekrassov V. 2005. Vinpocetine blockade of sodium channels inhibits the rise in sodium and calcium induced by 4-aminopyridine in synaptosomes. *Neurochem Int.* 46:533–540.
- Sitges M, Nekrassov V. 1999. Vinpocetine selectively inhibits neurotransmitter release triggered by sodium channel activation. *Neurochem Res.* 24:1585–1591.
- Siuciak JA, McCarthy SA, Chapin DS, Reed TM, Vorhees CV, Repaske DR. 2007. Behavioral and neurochemical characterization of mice deficient in the phosphodiesterase-1B (PDE1B) enzyme. *Neuropharmacology.* 53:113–124.
- Snyder GL, Prickaerts J, Wadenberg ML, Zhang L, Zheng H, Yao W, Akkerman S, Zhu H, Hendrick JP, Vanover KE, et al. 2016. Preclinical profile of ITI-214, an inhibitor of phosphodiesterase 1, for enhancement of memory performance in rats. *Psychopharmacology (Berl).* 233:3113–3124.
- Staley KJ, Otis TS, Mody I. 1992. Membrane properties of dentate gyrus granule cells: comparison of sharp microelectrode and whole-cell recordings. *J Neurophysiol.* 67:1346–1358.
- Surmeier DJ, Ding J, Day M, Wang Z, Shen W. 2007. D1 and D2 dopamine-receptor modulation of striatal glutamatergic signaling in striatal medium spiny neurons. *Trends Neurosci.* 30:228–235.
- Surmeier DJ, Plotkin J, Shen W. 2009. Dopamine and synaptic plasticity in dorsal striatal circuits controlling action selection. *Curr Opin Neurobiol.* 19:621–628.
- Thestrup T, Litzlbauer J, Bartholomaeus I, Mues M, Russo L, Dana H, Kovalchuk Y, Liang Y, Kalamakis G, Laukat Y, et al. 2014. Optimized ratiometric calcium sensors for functional in vivo imaging of neurons and T lymphocytes. *Nat Methods.* 11:175–182.
- Threlfell S, West AR. 2013. Review: modulation of striatal neuron activity by cyclic nucleotide signaling and phosphodiesterase inhibition. *Basal Ganglia.* 3:137–146.
- Valjent E, Bertran-Gonzalez J, Herve D, Fisone G, Girault JA. 2009. Looking BAC at striatal signaling: cell-specific analysis in new transgenic mice. *Trends Neurosci.* 32:538–547.
- Vallebuona F, Raiteri M. 1995. Age-related changes in the NMDA receptor/nitric oxide/cGMP pathway in the hippocampus and cerebellum of freely moving rats subjected to transcerebral microdialysis. *Eur J Neurosci.* 7:694–701.
- Vemulapalli S, Watkins RW, Chintala M, Davis H, Ahn HS, Fawzi A, Tulshian D, Chiu P, Chatterjee M, Lin CC, et al. 1996. Antiplatelet and antiproliferative effects of SCH 51866, a novel type 1 and type 5 phosphodiesterase inhibitor. *J Cardiovasc Pharmacol.* 28:862–869.
- Yan C, Bentley JK, Sonnenburg WK, Beavo JA. 1994. Differential expression of the 61 kDa and 63 kDa calmodulin-dependent phosphodiesterases in the mouse brain. *J Neurosci.* 14:973–984.
- Yapo C, Nair AG, Clement L, Castro LR, Hellgren Kotaleski J, Vincent P. 2017. Detection of phasic dopamine by D1 and D2 striatal medium spiny neurons. *J Physiol.* 595:7451–7475.